Step Dipole Moment and Step Line Tension on Au(100) in aqueous KBr electrolyte

Mohammad Al-Shakran, Ludwig A. Kibler, Timo Jacob [1]

Guillermo L. Beltramo[2] and Margret Giesen[3*]

[1]*Institut für Elektrochemie, Universität Ulm, Albert-Einstein-Allee 47, 89081 Ulm, Germany.*

[2]*Institute of Complex Systems (ICS-7), Jülich Forschungszentrum GmbH, 52425 Jülich, Germany.*

[3]*Peter Grünberg Institute (PGI-6), Jülich Forschungszentrum GmbH, 52425 Jülich, Germany.*

Abstract:

Here, we demonstrate a new method to measure step dipole moments for electrode surfaces in the presence of specifically adsorbed anion adlayers. The method is based on potential-dependent studies of the equilibrium shape and the equilibrium fluctuations of monatomic high Au islands as observed in scanning tunneling microscopy data.

Furthermore we measure the angular anisotropy of the absolute step line tension for an Au(100) electrode in contact with KBr solution. A method previously introduced for surfaces in vacuum is now extended for electode surfaces in contact with electrolyte.

* **Corresponding author.** Email: m.giesen@fz-juelich.de;
http://www.fz-juelich.de/SharedDocs/Personen/PGI/PGI-6/EN/Giesen_M.html?nn=545850

1. Introduction

In order to understand the behaviour of electrochemical interfaces and in order to gain a better knowledge of the effective parameters related to the performance of energy storage devices, detailed knowledge of elementary processes at electrode surfaces on an atomistic level is of great importance. Fundamental studies of atomic diffusion phenomena, degradation and corrosion at the atomic scale have therefore attracted quite some interest in recent years [1-4]. Particular interest has been focused on the quantitative analysis of atomic scale phenomena such as coarsening [5-9], corrosion [10-12] and deposition [13-19]. Some of the work contributed by measuring energetic parameters such as kink energies [4, 20-23], step line tension values for atomically dense directions [24-26] or the mean step line tension averaged over all crystal surface directions [22, 23, 27].

Other studies focused on the defect dipole moment that has a large linear contribution to the defect energy and diffusion barriers due to its interaction with the strong electric field across the double layer [28] and may therefore also have an influence on charge carrier transport across the electrode-electrolyte interface. The linear dependence of defect energies and diffusion barriers on the electrode potential is a general phenomenon and has been observed and quantitively described in many studies [4, 25, 26, 29-33]. Dipole moments of defects on electrode surfaces are of particular interest for understanding the physics and chemistry of electrodes on the atomic scale since they have a large influence on the electrode work function and lead to a shift in the potential of zero charge [34, 35]. Dipole moments per step atom can be experimentally deduced from this shift [25, 26, 36, 37].

In addition, the dipole moment of defects leads to an exponential increase of transport rates on electrode surfaces [4, 20, 28, 33, 38-40]. Dipole interactions between adsorbed species on electrode surfaces may considerably influence the surface stress [41]. Furthermore it has been discussed previously that dipole moments of lattice vacancies have a major impact on the performance of perovskite oxides as electrode materials [30]. Therefore, measuring the dipole moments of defects is a major contribution towards understanding electrode surfaces at the atomic scale.

Here, we propose a new method to measure step dipole moments. We follow an approach recently demonstrated for the dipole moments of kinks [4] where the dipole moment of the kink is directly deduced from the potential dependence of the kink energy.

For that purpose, we measure the step line tension as a function of the electrode potential by analyzing shape fluctuations of monolayer high islands on the electrode surface. From the potential dependence we obtain a value for the dipole moments of step edges. In this work, the behavior of an Au(100) electrode in contact with an aqueous KBr solution has been studied. Similar studies could be likewise performed however for other systems.

Whereas the analysis of island shape fluctuations merely yields the mean step line tension averaged along the island perimeter and hence, a mean step dipole moment, information on the angular anisotropy of the step line tension is still lacking. Therefore, we explore for the first time the full crystal anisotropy of the step line tension in electrolye environment by means of a method previously applied to surfaces in vacuum [42-44].

This paper is organized as follows: The next section describes the experimental and theoretical procedures. We present our experimental results in Section 3. This part is followed by the discussion in Section 4. The paper closes with a summary in Section 5.

2. Experimental procedures and methods

2.1 Scanning tunneling microscopy, electrolyte and sample preparation

The scanning tunneling microscopy (STM) measurements were performed using the electrochemical version of the Topometrix TMX 2010 discoverer instrument. The potentials of the tip and the Au sample were controlled independently by a bipotentiostat. All experimental results were obtained at room temperature.

The STM tips used in the experiments were etched electrochemically from polycrystalline tungsten wires and coated with an electrophoretic paint to minimize Faraday currents at the foremost part of the tip. All STM images were recorded in constant-current mode (I_t= 2 nA) with 500 x 500 pixel resolution.

High purity polycrystalline annealed Pt wires (Goodfellow, 99.999%) served as counter and quasi-reference electrodes in the STM cell. In the following, electrode potentials are given with respect to the saturated calomel electrode (SCE).

The electrolytes were prepared with H_2SO_4 (Merck, suprapure), KBr (Aldrich, 9.995%) and ultrapure water (18.2 MΩ cm, total oxidizable carbon <1 ppb).

For STM measurements of the island shape, we used a Au(100) disk (12 mm diameter and 2 mm thickness) (MaTecK - Jülich, Germany), which was cut and prepared by spark erosion from a single crystal rod. Prior to each experiment, the Au(100) single crystal was annealed for 5 min at about 900°C and cooled down to room temperature in an Argon atmosphere. The crystal was subsequently mounted in the STM cell which was connected to the bipotentiostat. The crystal surface was then brought in contact with the electrolyte under potential control at potentials below the potential of zero charge (pzc).

For voltammetry measurements, a smaller Au(100) single crystal (4 mm thickness and 4 mm diameter) was used. The preparation of the gold electrode prior experiments followed the same procedure as that for the STM measurements described above. The Au(100) single crystal was brought in contact with the electrolyte under potential control at values below pzc. The contact between the electrode surface and the electrolyte was done by the hanging meniscus method [45]. A saturated calomel electrode and a platinum wire served as a reference and counter electrode, respectively.

For the experimental analysis, the monatomic high Au islands were created by stepping the electrode potential from negative values, where the electrode surface is reconstructed (hex-reconstruction), to higher potentials where the surface reconstruction is lifted and the (1x1) surface emerges [46-48].

Fig. 1(a) shows the cyclic voltammogram (scanrate 10 mV s^{-1}) as obtained for the electrode samples used in our experiments for the electrolyte of interest. Four of the potentials considered in this study lie between the lifting of the quasi-hex Au(100) surface reconstruction [49] indicated by the current peak peak around -0.1 V in the cyclic voltamogram and the formation of an ordered $c\left(\sqrt{2} \times 2\sqrt{2}\right)R45°$ Br adlayer around +0.12 V [50]. The data points at +0.11 and 0.17 V are located nominally in the regime of the ordered adlayer.

In addition to the voltammetry data, we have plotted in Fig. 1(b) the surface charge density of Au(100) in 9 mM $KClO_4$ + 1mM KBr as previously published in [4]. Here, we have restricted the surface charge density data to the potential range where the STM measurements in this study have been performed. The surface charge density data in Fig. 1(b) is later used to

interpret the data for the step line tension as measured versus the electrode potential in terms of the surface charge density (see discussion in chapter 4).

2.2 Image processing codes

The STM images were analyzed using a homemade image processing code based on MatLab® (version 7.11.0 R2010b, Mathworks Inc). The raw STM images were first leveled using a standard polynominal line-by-line leveling procedure to enhance the dynamic range of the image contrast ([51]; *pp.* 238 “Fitting a background function”). A 3x3 median filter was applied to decrease noise in the image. For the STM images used in this work, this median filter did not cause any measurable changes in the island perimeter within the pixel resolution of the image. A circular mask was positioned around the island. Starting from the center of the mask the image grey scale values of the pixels along radial lines were fitted to polynominal functions. The largest slope in the polynominal fit defined the island edge. Noise in the grey scale values might lead to non-physical values for the island edge position. This was accounted for by neglecting unphysically large jumps in the island edge position. In these cases, the island edge position at the respective radial line was defined as the position found for the neighbor line determined previously. Finally, the deduced island perimeter was controlled visually to avoid errors.

The mean island shape was determined by scaling all individual island perimeters to the same island area. Island fluctuations were finally analyzed calculating the deviation of an individual island shape from the mean shape by simultaneously sorting the individual island shapes into packages of similar island radius.

2.3 Theoretical methods

Following procedures described in detail in refs. [42, 52-54], the step line tension is measured using a capillary wave analysis of the island perimeter fluctuations around a mean shape. This method has successfully been applied to many systems in vacuum for substrates of low anisotropy [42, 53-55], substrates with high anisotropy [43, 56] as well as in electrolyte [22, 23, 27]. In this report, we merely repeat the final equations used here. For details we refer to previously published papers [42, 44, 52-54, 57].

The mean step line tension $\bar{\beta}$ is given by the time-averaged fluctuation function:

$$\langle G(r)\rangle_t = \frac{3k_B T\,\bar{r}}{4\pi\bar{\beta}} \tag{1}$$

Here, $\bar{r}$ is the mean radius of the island averaged along its perimeter and the step line tension $\bar{\beta}$ represents the average along the island perimeter. Hence, from eq. (1) one does not obtain the anisotropy of the step line tension for different crystal directions. As has been demonstrated in [42-44], the anisotropy can be determined, however, from the following equation:

$$\frac{\bar{\beta}}{\beta_0} = \frac{1}{2\pi}\int_0^{2\pi}\left[\frac{\frac{\beta(\theta_p)}{\beta_0}}{\frac{\bar{r}}{r_0^4}}\frac{\frac{r^4(\theta_p)}{r_0^4}}{\left[r^2(\theta_p)+\frac{\partial r(\theta_p)}{\partial\theta_p}\right]^{3/2}}\right]d\theta_p \tag{2}$$

.

In eq. (2), β_0 and r_0 are the step line tension and the island radius at polar angle $\theta_p = 0$, i.e. for steps oriented along the atomically dense ⟨110⟩- direction. $\beta(\theta_p)$, $r(\theta_p)$ denote the anisotropy of the step line tension and the island radius vs. θ_p.

Eq. (2) is a tool to determine absolute values of the step line tension: $r(\theta_p)$, r_0 and $\frac{\partial r(\theta_p)}{\partial \theta_p}$ are directly deduced from a polar plot of the measured island equilibrium shape. $\frac{\beta(\theta_p)}{\beta_0}$ is obtained from the island equilibrium shape via an inverse Wulff construction [58]. As a caveat we note that the inverse Wulff construction yields $\frac{\beta(\theta_t)}{\beta_0}$ with θ_t the tangential angle rather than the polar angle θ_p (for details on the geometrical difference between these angles we refer to [43, 44]). As has been discussed in [43], there is, however, a simple relation between both angles [59] that can be used to evaluate eq. (2):

$$\theta_p = \theta_t + atan\left[\frac{\frac{d\beta(\theta_t)}{d\theta_t}}{\beta(\theta_t)}\right]. \qquad (3)$$

Since $\bar{\beta}$ is obtained from island shape fluctuations in a certain temperature and potential range, the ratio $\beta(\theta_p)/\beta_0$ is generally a temperature and potential dependent function. In our experiments though, *T*=297 K is constant and the electrode potential E varies between -0.08 and +0.17 V vs. SCE. For small anisotropy and little variation of $\beta(\theta_p)$ with temperature and electrode potential (as is the case of bromide on Au(100) (see later in Fig. 6(a)), it suffices to evaluate eq. (2) with data for $\beta(\theta_p)/\beta_0$ at a single intermediate temperature/potential [42]. In the study presented here, however, we have used the potential-dependent value of $\bar{\beta}$ as measured (Fig. 5) to calculate eq. (2). Finally we emphasize that the determination of the anisotropy of the step line tension via eq. (2) is valid only if first, the 2D-equilibrium island shape has no facets, i.e. the Wulff plot has no cusp. Secondly, island edges must retain the same sign of the curvature along their perimeter.

3. Results

Fig. 2 shows STM images of Au(100) in 0.05 M H_2SO_4 + 1 mM KBr at (a) -0.06 V and (b) +0.17 V vs. SCE. At these potentials the surface reconstruction of the clean Au(100) electrode is lifted and monatomic high islands nucleate on the surface [60]. The islands are mobile and undergo coarsening [2] and island edge fluctuations.

We have analyzed equilibrium shape islands displayed in STM images similar to those shown in Fig. 2 for potentials -0.08, -0.06, 0, +0.05, +0.11 and +0.17 V vs. SCE. At +0.17 V, the highest potential used, which is nominally above the transition to an ordered $c\left(\sqrt{2} \times 2\sqrt{2}\right)R45°$ bromide adlayer (see Fig. 1) [50], some islands slightly deviate from the square shape. As an example we have marked an individual island in Fig. 2(b).

We concluded that this shape deviation is due to the onset of formation of an ordered bromide adlayer. Since the formation of an ordered adlayer structure considerably influences the equilibrium shape and the corresponding line tension, we did not consider these island shapes for our analysis.

Fig. 3(a) shows the equilibrium shape $r\left(\theta_p\right)$ for the various potentials in a polar plot. The corresponding Wulff plots $\frac{\beta(\theta_t)}{\beta_0}$ are displayed in Fig. 3(b). The islands reflect the square symmetry of the substrate but the island edges are considerably rounded. A measure for the rounding of the island corners is the aspect ratio $\frac{\beta(45°)}{\beta_0}$. For a perfect square, $\frac{\beta(45°)}{\beta_0} = \sqrt{2}$, for a perfect circle $\frac{\beta(45°)}{\beta_0} = 1$ [57]. From the Wulff plot in Fig. 3(b) we find for Au(100) in 0.05 M H_2SO_4 + 1 mM KBr a maximum aspect ratio around $\frac{\beta(45°)}{\beta_0} = 1.16$, 16% larger than 1.

We have measured the fluctuation function $\langle G(r)\rangle_t$ as the deviation of individual island shapes from the equilibrium shape (Eq. (1)) at the potentials given before. The data is shown

in Fig. 4. The fluctuations increase with increasing electrode potential. In order to determine the mean step line tension we assume first, eq. (1) is valid and that a linear fit to the data is justified. Second we use the strict boundary condition $\langle G(\bar{r}=0)\rangle_t = 0$. This is an important assumption since it contributes to the data set without any experimental error bar and therefore influences significantly the determined linear slope, respectively the value of the mean step line tension. The obtained linear fits are plotted in Fig. 4(a)-(f) as solid lines. From the respective slopes we obtain values for the mean step line tension $\bar{\beta}$ as indicated in the view graphs. $\bar{\beta}$ decreases with increasing electrode potential. In order to visualize the potential dependence of the mean step line tension, we have plotted $\bar{\beta}$ vs. electrode potential in Fig. 5(a). The mean step line tension depends linearily on the electrode potential. The respective plot of $\bar{\beta}$ vs. the surface charge density is shown in Fig. 5(b). Obviously, $\bar{\beta}$ is also in accordance with a linear dependence on the surface charge density. This is due to the fact that the surface charge density depends almost linear on the electrode ppotential in the considered potential range. In summary, the mean step line tension as measured in this work is in accordance with previous reports [28, 33, 40] that defect energies should linearily depend on the surface charge density.

The mean step line tension reflects merely the average of the step line tension along the island perimeter rather than the angular anisotropy of the step line tension β. According to eq. (2), absolute values for the step line tension can be determined by means of the equilibrium shape and the respective Wulff plot obtained from an inverse Wulff construction [44, 58] as plotted in Fig. 3 (a) and (b).

The anisotropy of the absolute step line tension for Au(100) in 0.05 M H_2SO_4 + 1 mM KBr is displayed in Fig. 6(a). Obviously, the anisotropy is quite small: from $\theta_p = 0°$ to 45° $\beta(\theta_p)$

varies about $\sim 9-15\%$ for all potentials in accordance with the Wulff plot presented in Fig. 3(b).

4. Discussion

From Fig. 5 we find that the step line tension in KBr solution depends linearily on the surface charge density as already proposed in [28, 33]. It was shown in these references that the defect dipole moment in the electric field of the double layer gives rise to an additional energy contribution to the defect energy. This contribution has a linear dependence on the surface charge density:

$$\beta(E) = \beta\left(E_{pzc}\right) - \frac{\mu_{step}}{\varepsilon_0}\sigma(E) \qquad (4)$$

Here, μ_{step} is the step dipole moment, ε_0 the vacuum permittivity, E_{pzc} the potential of zero charge (*pzc*) and $\sigma(E)$ is the potential dependent surface charge density. From eq. (4) it follows that if one measures the defect energy as a function of the surface charge density, one can determine the related defect dipole moment. This method was previously successfully applied to determine the dipole moment of kinks in Br^- and Cl^-containing electrolytes [4]. Here, we demonstrate that the method also works for step dipole moments. The result for Au(100) in 0.05 M H_2SO_4 + 1 mM KBr is presented in Fig. 5(b): Experimental data for the mean step line tension vs. surface charge density is plotted as grey squares. The solid line is a linear fit to the data and the dashed lines reflect the uncertainty due to the fit error. From the slope of the fit we determine a step dipole moment of $\mu_{step} = (5.3 \pm 0.9) \times 10^{-3}\ e\text{Å}$. This value is comparable to previous data on the step dipole moment on stepped Au and Ag surfaces in various aqueous electrolytes [25, 26]. In Fig. 7 we compare our data in

KBr solution with previous data on the step line tension in sulfate and chloride containing electrolyte. In this plot we have used surface charge density data as measured in 0.5 M H_2SO_4, respectively in 0.01 M $HClO_4$ + 1 mM HCl [61].

Independent of the nature of the electrolyte anion, the data sets collapse with approximately the same linear dependence on the surface charge density. However, for the HCl and H_2SO_4 electrolyte the data points at lowest and highest potential deviate considerable from the linear trend. In the case of chloride solution (circles in Fig. 7), this deviation might be caused by the fact that the electrode potential is close to the re-establishment of the surface reconstruction. For the sulfate solution (triangles in Fig. 7) the deviation might arise because the electrode potential is close to the oxidation potential of the gold electrode.

If one neglected these data points a linear fit to the HCl and H_2SO_4 electrolyte data would approximately yield a similar slope compared to the KBr data and hence to a similar step dipole moment in accordance to previous data where the step dipole moment was determined from impedance spectroscopy data [26].

A collapse of the data with approximately the same step dipole moment independent on electrolyte corroborates also previous data on Ag surfaces. Beltramo et al. showed that the polarizability does not depend on the electrolyte anion over a large potential range [62]. This is an interesting result and requires further thinking. It seems as if the mean step line tension and the step dipole moment are mainly determined by the surface charge density of the electrode surface rather than by the electrode material or by the type of the electrolyte anion. In this context the collapse of the dipole moments and the values for $\bar{\beta}$ for Au(100) in Br^-, Cl^- and SO_4^{2-} electrolytes as considered here can be understood: The surface charge

density curves on Au electrodes show a quite similar dependence on the electrode potential, safe for the shift in the potential of zero charge [4, 63]. Hence, one would also expect a similar value of the step dipole moment for the three electrolytes.

As a caveat we mention that for the data as presented in this work for KBr solution the data point at +0.17 V is located in the potential regime between two sharp transition peaks at +0.12 and +0.5 V in the *i-E* curve (Fig. 1(a)). According to reference [50], the first peak at +0.12 V is related to the formation of an ordered $c(\sqrt{2} \times 2\sqrt{2})R45°$ bromide adlayer. The second peak indicates the transition to an uniaxially incommensurate $c(\sqrt{2} \times p)R45°, 2\sqrt{2} \geq p \geq 2.5$ bromide adlayer [64]. It has been shown in [50] that islands assume trigonal symmetry when the $c(\sqrt{2} \times 2\sqrt{2})R45°$ structure is formed. In our experiments however, most of the islands resemble the square symmetry of the Au(100) substrate reflected in the square shape of the equilibrium shape in Fig. 3(a). Only a minor amount of islands show island segments along crystallographic directions in accordance with a trigonal symmetry (marked island in Fig. 2(b)). We assume therefore that – despite the nominal potential of 0.17 V – the $c(\sqrt{2} \times 2\sqrt{2})R45°$ adstructure has not been fully established yet and that the real electrode potential is lower than the nominal one. This is a reasonable assumption since we used Pt wires as quasi-reference electrodes in our STM studies which are known to be unstable. The typical error in electrode potential lies in the range of $\pm$0.05 V. This error in the electrode potential gives rise to likewise small error bars in the surface charge density as indicated in Fig. 5(b) for surface charge density axis.

We did not perform systematic measurements of the surface coverage with bromide for a given potential. However, from the surface charge density measurements [4] we deduce that our STM data was obtained for bromide coverages between 0.25 and 0.5 ML, in

accordance with the observation that the full bromide adlayer has not been yet established. Since some island shapes deviate from the square symmetry, we assume that the data obtained at +0.17 V were obtained at coverages $\lesssim$ 0.5 ML. Hence, we can safely deduce that the step dipole moment of $\mu_{step} = (5.3 \pm 0.9) \times 10^{-3}\ e\text{Å}$ is the dipole moment of Au(100) steps in the presence of a considerable amount of bromide on the electrode surface, however, not in the presence of an fully ordered bromide adlayer.

The anisotropy of the step line tension as shown here might be compared to previous data as measured for metal surfaces in vacuum: On Pt(111) for instance, islands have an equilibrium shape similar to truncated islands due to the fcc (111) symmetry of the surface. The equilibrium shape contains two different step types, A and B, with (100), respectively (110) microfacets at the step edge. A- and B-steps are oriented along $\langle 2\bar{1}\bar{1} \rangle$ and $\langle 11\bar{2} \rangle$ with an angle of 60° between them. Hence, the anisotropy is measured between polar angles 0° and 60°. For Pt(111), an anisotropy of about 16 % was found [43]. For Cu(111) [53], the anisotropy is smaller. Here, A-steps have a 1% higher energy than B-steps. For fcc (100) surfaces in vacuum, the anisotropy of step energies were determined only for Cu(100) so far. Here, an anisotropy of about 13% for island edges along $\langle 110 \rangle$ and $\langle 100 \rangle$ was found. Both values are comparable with the result we find for Au(100) in KBr. The absolute values for the step energy, however, differ considerably: For Cu(100) in vacuum the mean step energy along the island perimeter is of the order of 220 meV per atom [57] and for Pt(111) with $a_{||}\beta_A$= 348±16 meV $a_{||}\beta_B$ = 300±14 meV [43].

Further data on the equilibrium shape and the Wulff plot have been previously published by the Jülich group for islands on Au(100) electrodes in H_2SO_4 [5, 22, 23] and in HCl solution [27, 65]. For Au(100) in 0.05 M H_2SO_4, aspect ratios $\beta_{45°}/\beta_0 \lesssim 1.10$ were measured. For Au(100)

in 1mM HCl, one deduces from the island shapes as published in [65] aspect ratios between 1.04 and 1.06 between 0 and 0.4 V SCE. Those results are similar although slightly smaller than what is found for Au(100) in KBr in this work.

In previous studies of Au(100) in H_2SO_4 and in HCl, no data on the absolute step line tension and its dependence on the crystallographic direction was reported. However, one may use the island equilibrium shapes, the Wulff plots as well as the respective values for the mean step line tension $\bar{\beta}$ as published in [22, 27, 65] to obtain information on the anisotropy of the absolute step line tension for dilute H_2SO_4 and HCl solutions by applying eq. (2). The respective results for some electrode potentials are shown in Fig. 6(b), (c). Here, the crystal anisotropy of the step line tension between 0 and 45° in the considered potential range is comparable to what is observed in KBr solution as presented in this work.

5. Summary

In summary, we have studied the island equilibrium shape and the island perimeter fluctuations for monatomic high islands on Au(100) in bromide-containing electrolyte. From the data we find absolute values of the step line tension β between 31 and 11 meV per atom in a $\langle 110 \rangle$-oriented step edge in a potential range between -0.08 and +0.17 V vs. SCE, respectively. Furthermore we analyzed the anisotropy of the step line tension with respect to the step edge orientation. For step orientations between the atomically dense $\langle 110 \rangle$-direction and the $\langle 100 \rangle$-orientation of a 100% kinked step we find anisotropies of the step line tension between 9 and 15% depending on the electrode potential considered in this work.

Finally by measuring the step line tension as a function of the surface charge density we deduced the step dipole moment $\mu_{step} = (5.3 \pm 0.9) \times 10^{-3}\ e\text{Å}$ in accordance with previous data for Au and Ag surfaces.

Acknowledgements

TJ and MG thank the financial support from the DFG (Deutsche Forschungsgemeinschaft). TJ additionally acknowledges financial support from the European Research Council through the ERC-StartingGrant THEOFUN (Grant Agreement No. 259608).

Figure Captions:

Fig. 1: (a) Cyclic voltammogram for Au(100) in 0.05 M H_2SO_4 + 1 mM KBr. Dashed lines indicate electrode potentials, which were used for the STM measurements. (at -0.08, -0.06, 0, +0.05, +0.11 and +0.17 V vs. SCE). Scanrate: 10 mV s^{-1}. (b) Surface charge density data as measured for Au(100) in 9 mM $KClO_4$ + 1mM KBr and previously published in [4]. Here, the data is restricted to the potential range where the STM measurements in this study have been performed.

Fig. 2: STM images of Au(100) in 0.05 M H_2SO_4 + 1 mM KBr at (a) -0.06 V and (b) +0.17 V vs. SCE. In (b) a particular island is marked by an arrow. The shape of this island obviously deviates from the square shaped islands in (a), an observation made for some islands at +0.17 V vs. SCE.

Fig. 3: (a) Island equilibrium shape as measured on Au(100) in 0.05 M H_2SO_4 + 1 mM KBr for various potentials. (b) Wulff-plot as determined from the equilibrium shape by an inverse Wulff construction [58]. Note, the Wulff plot is given with respect to the tangential angle θ_t that is related to the polar angle θ_p via eq. (3) [59]. All potentials are given with respect to SCE.

Fig. 4: Island fluctuation function$\langle G(\bar{r})\rangle_t$ measured at (a) -0.08 V, (b) -0.06 V, (c) 0 V, (c) +0.05 V, (e) +0.11 V and (f) +0.17 V (all potentials with respect to SCE). The lines are weighted linear fits to the data assuming eq. (1) is valid. In addition, we used the strict additional boundary condition $\langle G(\bar{r}=0)\rangle_t = 0$. The number of data points in each view graph is determined by the width of the size distribution of the analyzed islands in the STM

images at a given electrode potential rather than by the total number of islands used for analysis.

Fig. 5: (a) Mean step line tension $\bar{\beta}$ vs. electrode potential as obtained determined in Fig. 4 from the perimeter fluctuations of monolayer high Au islands on Au(100) in 0.05 M H_2SO_4 + 1 mM KBr. (b) The same data for $\bar{\beta}$ as plotted vs. the surface charge density as previously reported in [4]. Here, we have used Fig. 1(b) to express the electrode potential in terms of surface charge density. The solid line is a linear fit to the data. According to eq. (4), the slope is propotional to the step dipole moment. See text for further discussion

Fig.6: Absolute step line tension β vs. polar angle θ_p as obtained from the equilibrium shape and the Wulff plot in Fig. 3 and using eqs. (2), (3). Data is presented for islands on Au(100) in (a) 0.05 M H_2SO_4 + 1 mM KBr, in (b) 0.1 M $HClO_4$ + 1 mM HCl (as deduced from refs. [65], [27]) and in (c) 0.05 M H_2SO_4 (as deduced from ref. [22], see text for further discussion). The ordinates for (a) and (b) are identical. The scale of the ordinate in (c) is indicated on the right hand side of the view graph.

Fig. 7: Mean step line tension $\bar{\beta}$ vs. surface charge density as determined in this work for specifically adsorbed Br^- (light grey squares), Cl^- (dark grey circles) [27] and for SO_4^{2-} (grey triangles) [22, 23]. (For the Cl^- and the SO_4^{2-} data we used surface charge density data as measured in 0.05 M H_2SO_4 and in 0.01 M $HClO_4$ +1 mM HCl [61].)

References:

[1] Catalysis in electrochemistry : from fundamentals to strategies for fuel cell development Wiley, Hoboken, NJ, 2011.
[2] M. Giesen, Prog. Surf. Sci., 68 (2001) 1.
[3] Electrochemistry at the Nanoscale, Springer, 2009.
[4] M. Al-Shakran, G. Beltramo, M. Giesen, Phys. Chem. Chem. Phys., 16 (2014) 12143.
[5] S. Dieluweit, M. Giesen, J. Phys. Condens. Matter, 14 (2002) 4211.
[6] K. Kubo, N. Hirai, S. Hara, Appl. Surf. Sci., 237 (2004) 301.
[7] N. Hirai, M. Yamauchi, T. Tanaka, S. Hara, Science and Technology of Advanced Materials, 5 (2004) 115.
[8] D.M. Kolb, R. Ullmann, J.C. Ziegler, Electrochim. Acta, 43 (1998) 2751.
[9] P. Broekmann, M. Wilms, M. Kruft, C. Stuhlmann, K. Wandelt, J. Electroanal. Chem., 467 (1999) 307.
[10] O. Magnussen, Faraday Discuss., 121 (2002) 43.
[11] O.M. Magnussen, M.R. Vogt, Phys. Rev. Lett., 84 (2000) 357.
[12] F.A. Möller, O.M. Magnussen, R.J. Behm, Zeitschrift fur Physikalische Chemie, 208 (1999) 57.
[13] L.H.S. Gasparotto, N. Borisenko, N. Bocchi, S. Zein El Abedin, F. Endres, Phys. Chem. Chem. Phys., 11 (2009) 11140.
[14] M.S. Zei, K. Wu, M. Eiswirth, G. Ertl, Electrochim. Acta, 45 (1999) 809.
[15] G. Staikov, W.J. Lorenz, Zeitschrift fur Physikalische Chemie, 208 (1999) 17.
[16] T.P. Moffat, J. Phys. Chem. B, 102 (1998) 10020.
[17] U. Schmidt, S. Vinzelberg, G. Staikov, Surf. Sci., 348 (1996) 261.
[18] Z. Shi, S. Wu, J. Lipkowski, Electrochim. Acta, 40 (1995) 9.
[19] J. Hotlos, O.M. Magnussen, R.J. Behm, Surf. Sci., 335 (1995) 129.
[20] M. Giesen, D.M. Kolb, Surf. Sci., 468 (2000) 149.
[21] S. Baier, M. Giesen, Phys. Chem. Chem. Phys., 2 (2000) 3675.
[22] S. Dieluweit, H. Ibach, M. Giesen, Faraday Discuss., 121 (2002) 27.
[23] S. Dieluweit, M. Giesen, J. Electroanal. Chem., 524-525 (2002) 194.
[24] G. Beltramo, M. Giesen, H. Ibach, Electrochim. Acta, 54 (2009) 4305.
[25] G.L. Beltramo, H. Ibach, U. Linke, M. Giesen, Electrochim. Acta, 53 (2008) 6818.
[26] G.L. Beltramo, H. Ibach, M. Giesen, Surf. Sci., 601 (2007) 1876.
[27] E. Pichardo-Pedrero, M. Giesen, Electrochim. Acta, 52 (2007) 5659.
[28] M. Giesen, G. Beltramo, S. Dieluweit, J. Muller, H. Ibach, W. Schmickler, Surf. Sci., 595 (2005) 127.
[29] K. Pötting, N.B. Luque, P.M. Quaino, H. Ibach, W. Schmickler, Electrochim. Acta, 54 (2009) 4494.
[30] E. Cockayne, B.P. Burton, Phys. Rev. B, 69 (2004) 144116.
[31] J.F. Jia, K. Inoue, Y. Hasegawa, W.S. Yang, T. Sakurai, Phys. Rev., B 58 (1998) 1193.
[32] T. Tansel, O.M. Magnussen, Phys. Rev. Lett., 96 (2006) 026101.
[33] E. Pichardo-Pedrero, G. Beltramo, M. Giesen, Appl. Phys., A87 (2007) 461
[34] K. Besocke, B. Krahl-Urban, H. Wagner, Surf. Sci., 68 (1977) 39.
[35] H. Ibach, W. Schmickler, Phys. Rev. Lett., 91 (2003) 016106.
[36] A. Hamelin, L. Stoicoveciu, L. Doubova, S. Trasatti, Surf. Sci., 201 (1988) L498.
[37] A. Hamelin, J. Lecoeur, Surf. Sci., (1976) 771.
[38] M. Giesen, M. Dietterle, D. Stapel, H. Ibach, D.M. Kolb, Surf. Sci., 384 (1997) 168.
[39] N. Hirai, H. Tanaka, S. Hara, Appl. Surf. Sci., 130-132 (1998) 506.
[40] N. Hirai, K. Watanabe, S. Hara, Surf. Sci., 493 (2001) 568.

[41] H. Ibach, Electrochim. Acta, 45 (1999) 575.
[42] C. Steimer, M. Giesen, L. Verheij, H. Ibach, Phys. Rev. B, 64 (2001) 085416.
[43] J. Ikonomov, K. Starbova, H. Ibach, M. Giesen, Physical Review B (Condensed Matter and Materials Physics), 75 (2007) 245411.
[44] S. Kodambaka, S.V. Khare, I. Petrov, J.E. Greene, Surf. Sci. Rep., 60 (2006) 55.
[45] A. Hamelin, J. Electroanal. Chem., 386 (1995) 1.
[46] D.M. Kolb, G. Lehmpfuhl, M.S. Zei, J. Electroanal. Chem., 179 (1984) 289.
[47] A.S. Dakkouri, Solid State Ionics, 94 (1997) 99.
[48] O.M. Magnussen, J. Hotlos, R.J. Behm, N. Batina, D.M. Kolb, Surf. Sci., 296 (1993) 310.
[49] D.M. Kolb, J. Schneider, Surf. Sci., 162 (1985) 764.
[50] A. Cuesta, D.M. Kolb, Surf. Sci., 465 (2000) 310.
[51] J.C. Russ, The image processing handbook, 5th ed. ed., CRC Press, Boca-Raton, Fla., 2007.
[52] S.V. Khare, T.L. Einstein, Phys. Rev. B, 54 (1996) 11752.
[53] G.S. Icking-Konert, M. Giesen, H. Ibach, Phys. Rev. Lett., 83 (1999) 3880.
[54] D.C. Schlößer, L.K. Verheij, G. Rosenfeld, G. Comsa, Phys. Rev. Lett., 82 (1999) 3843.
[55] S. Kodambaka, S.V. Khare, V. Petrova, A. Vailionis, I. Petrov, J.E. Greene, Vacuum Selected papers revised from the Proceedings of the Seventh International Symposium on Sputtering and Plasma Processes (ISSP 2003), 74 (2004) 345.
[56] S. Kodambaka, V. Petrova, S.V. Khare, D.D. Johnson, I. Petrov, J.E. Greene, Phys. Rev. Lett., 88 (2002) 146101.
[57] M. Giesen, C. Steimer, H. Ibach, Surf. Sci., 471 (2001) 80.
[58] G. Wulff, Z. Kristallgr. Mineral., 34 (1901) 449.
[59] S. Dieluweit, H. Ibach, M. Giesen, T.L. Einstein, Phys. Rev. B, 67 (2003) R121410.
[60] J. Schneider, D.M. Kolb, Surf. Sci., 193 (1988) 579.
[61] G. Beltramo, unpublished, (2013).
[62] G. Beltramo, E. Santos, W. Schmickler, Langmuir, 19 (2003) 4723.
[63] J. Lipkowski, Z. Shi, A. Chen, B. Pettinger, C. Bilger, Electrochim. Acta, 43 (1998) 2875.
[64] B.M. Ocko, O.M. Magnussen, J.X. Wang, R.R. Adić, T. Wandlowski, Physica B: Condensed Matter, 221 (1996) 238.
[65] M. Giesen, AIP Conference Proceedings, 916 (2007) 115.

Figure 1

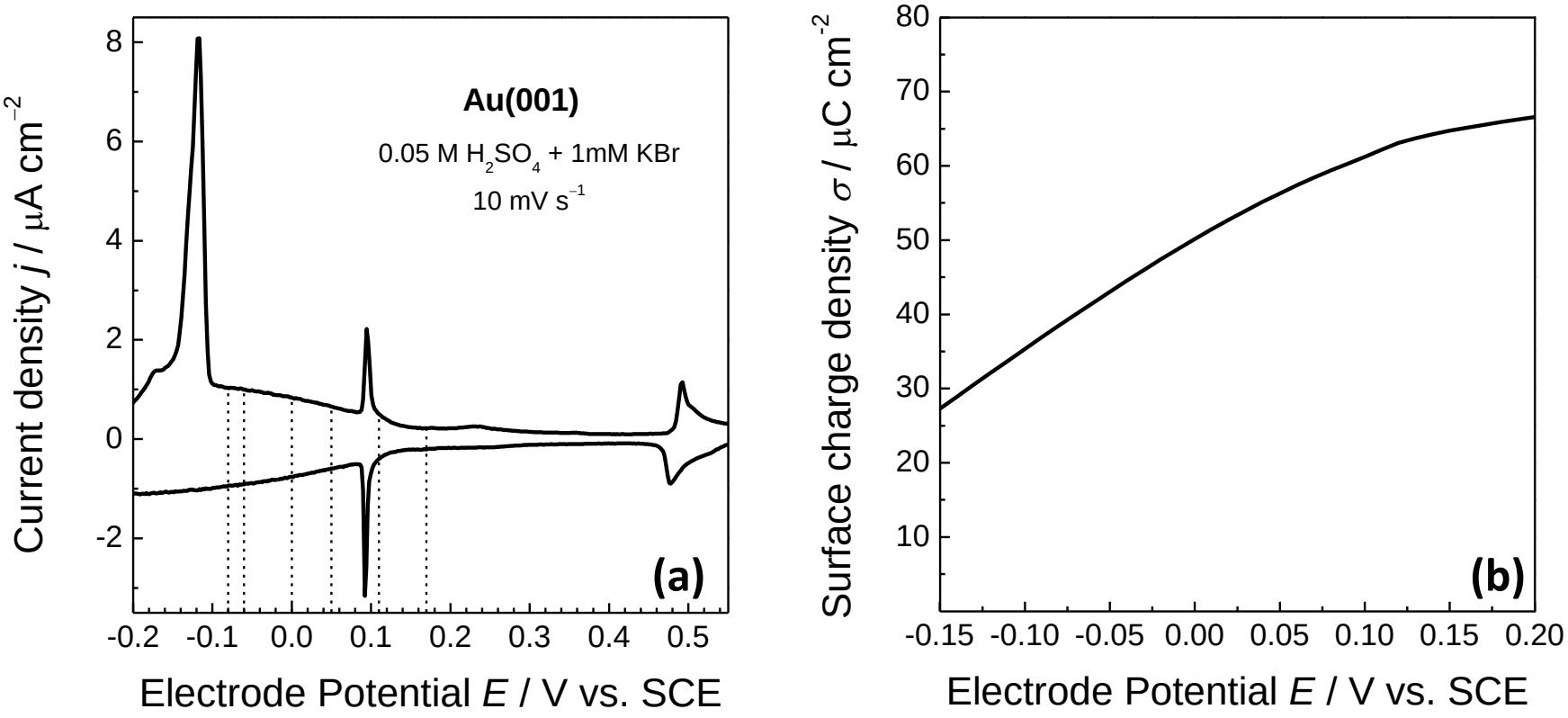

Fig. 1

Figure 2

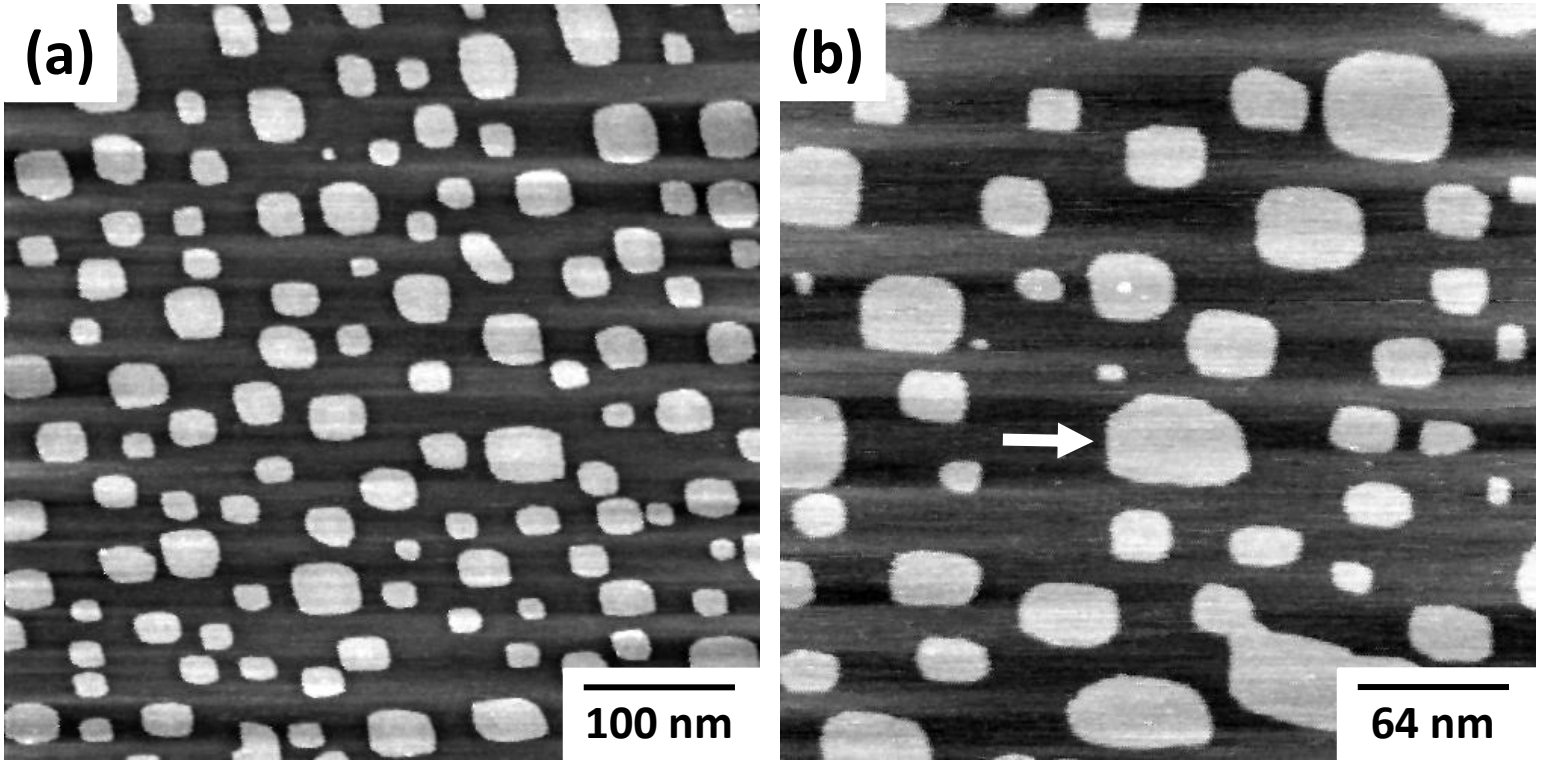

Fig. 2

Figure 3

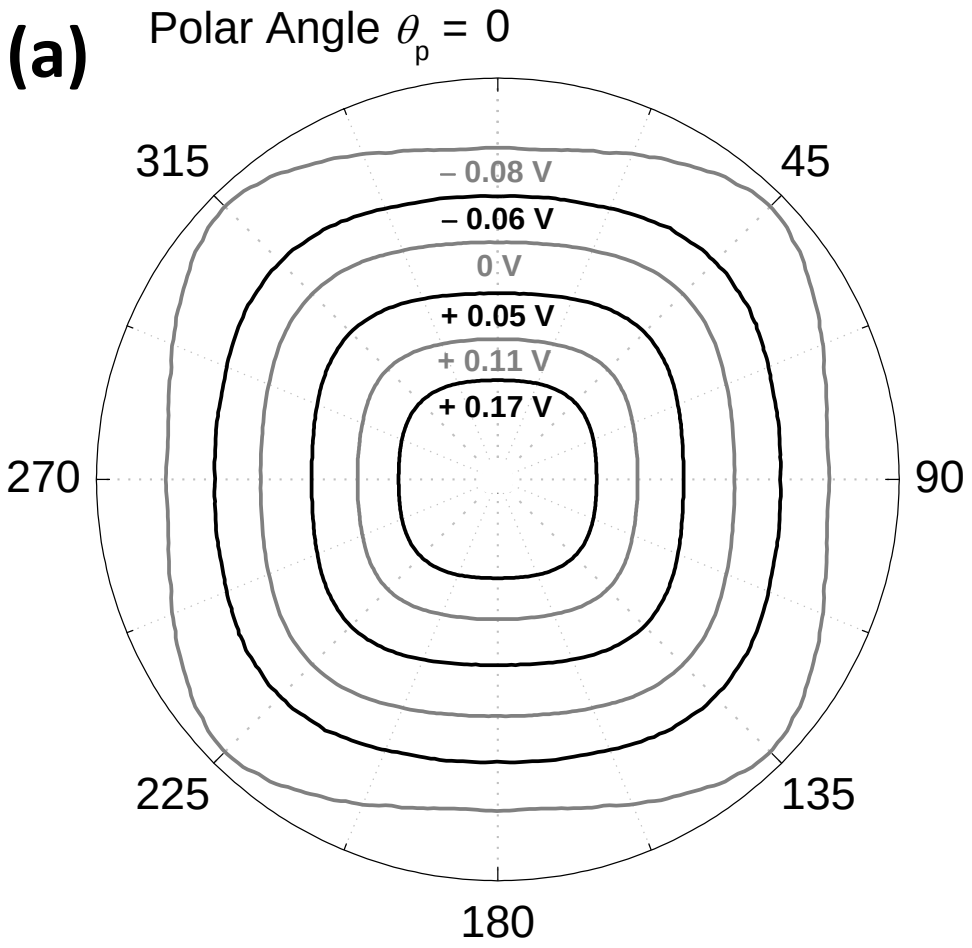

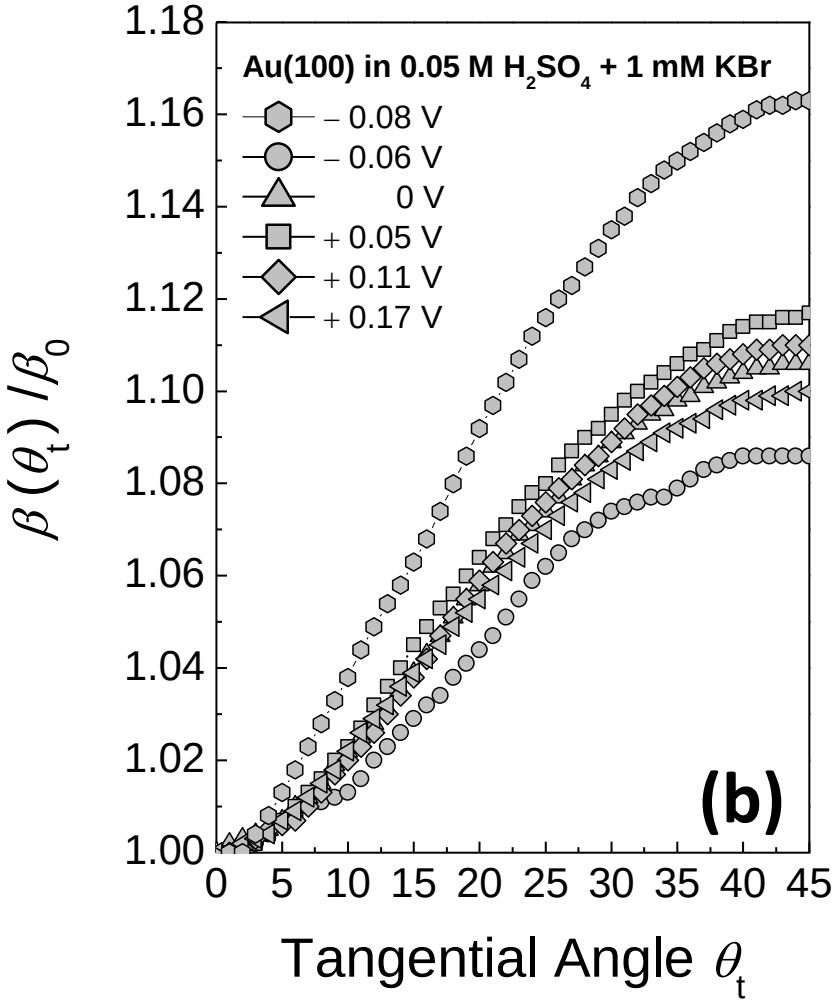

Fig. 3

Figure 4

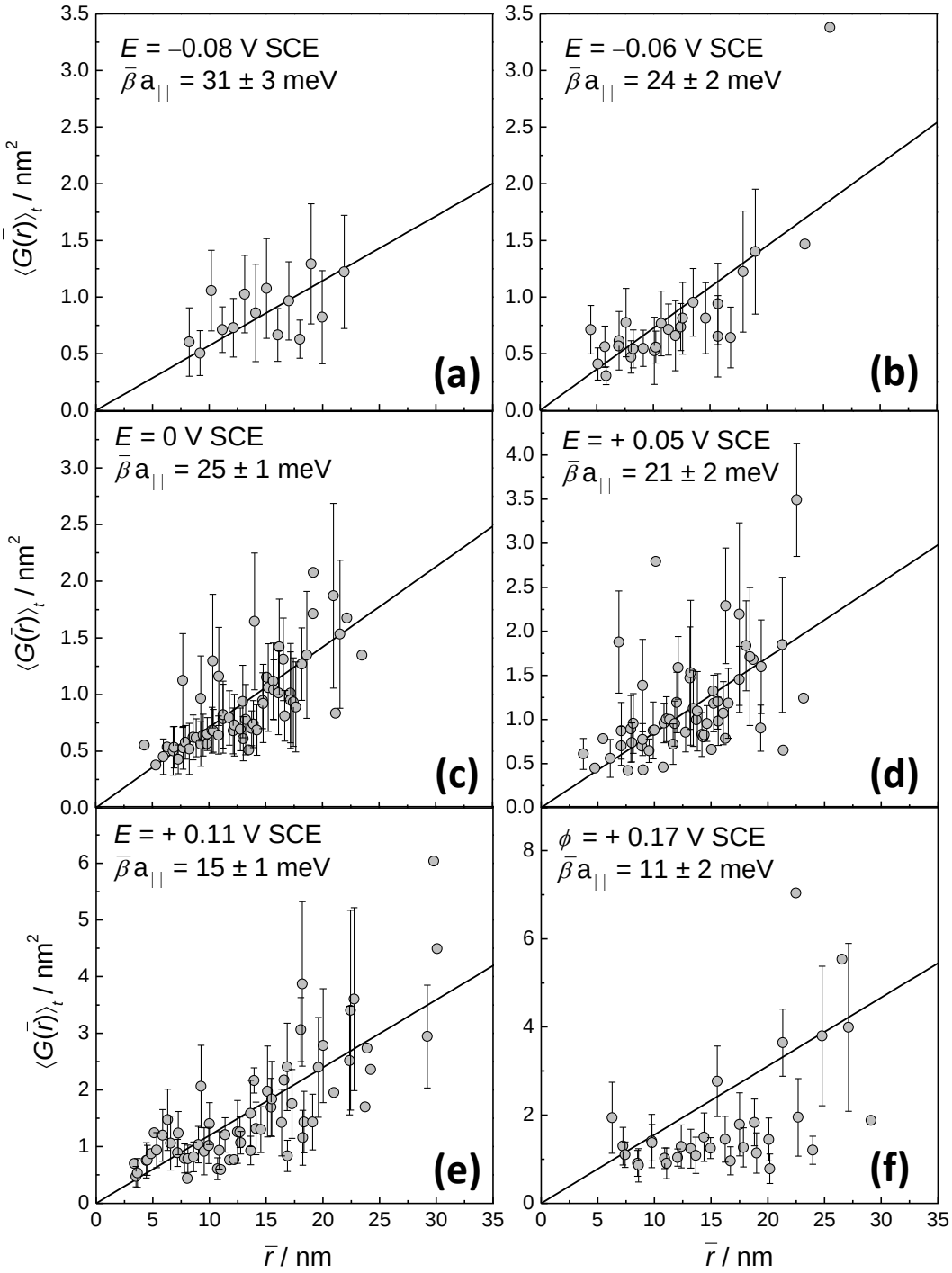

Fig. 4

Figure 5

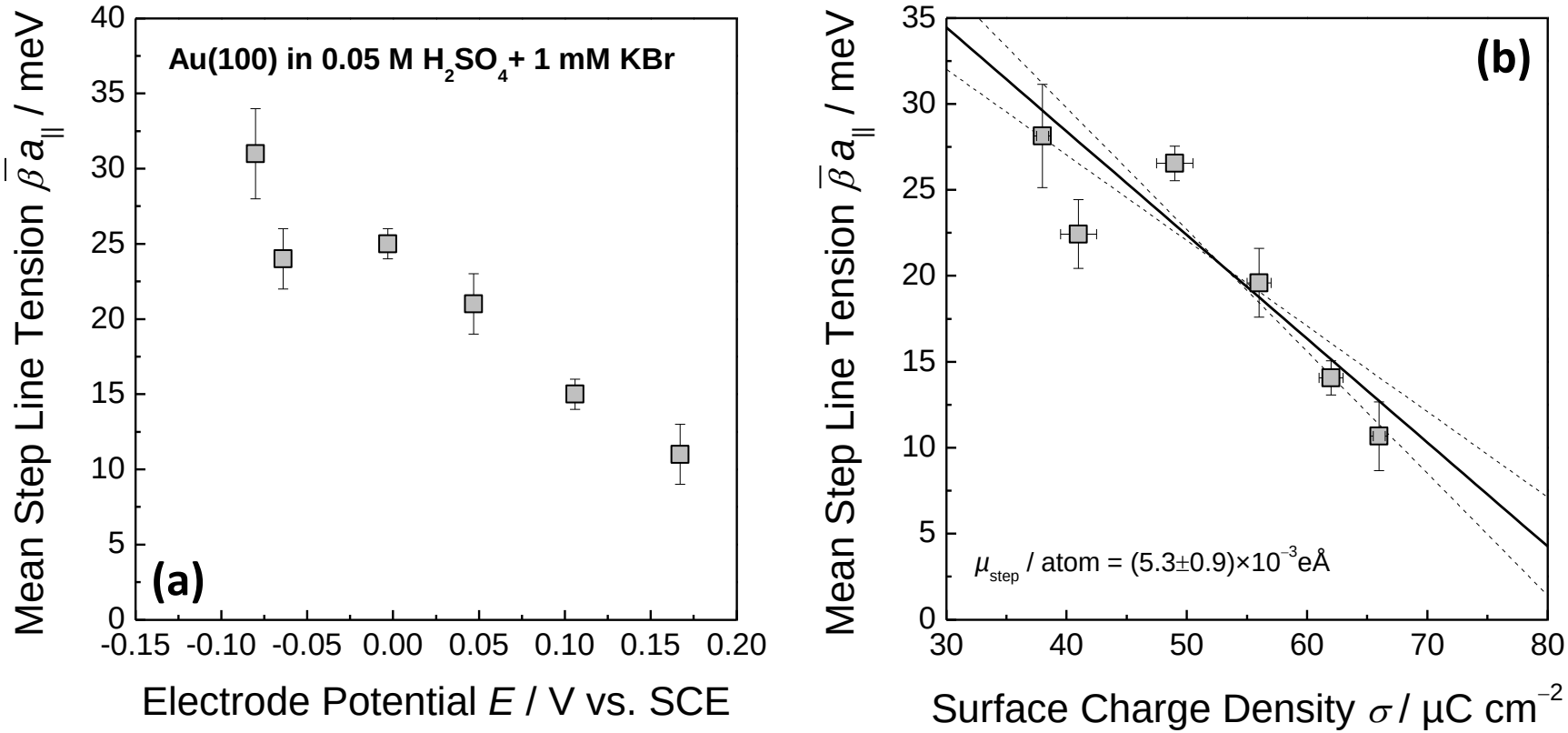

Fig. 5

Figure 6

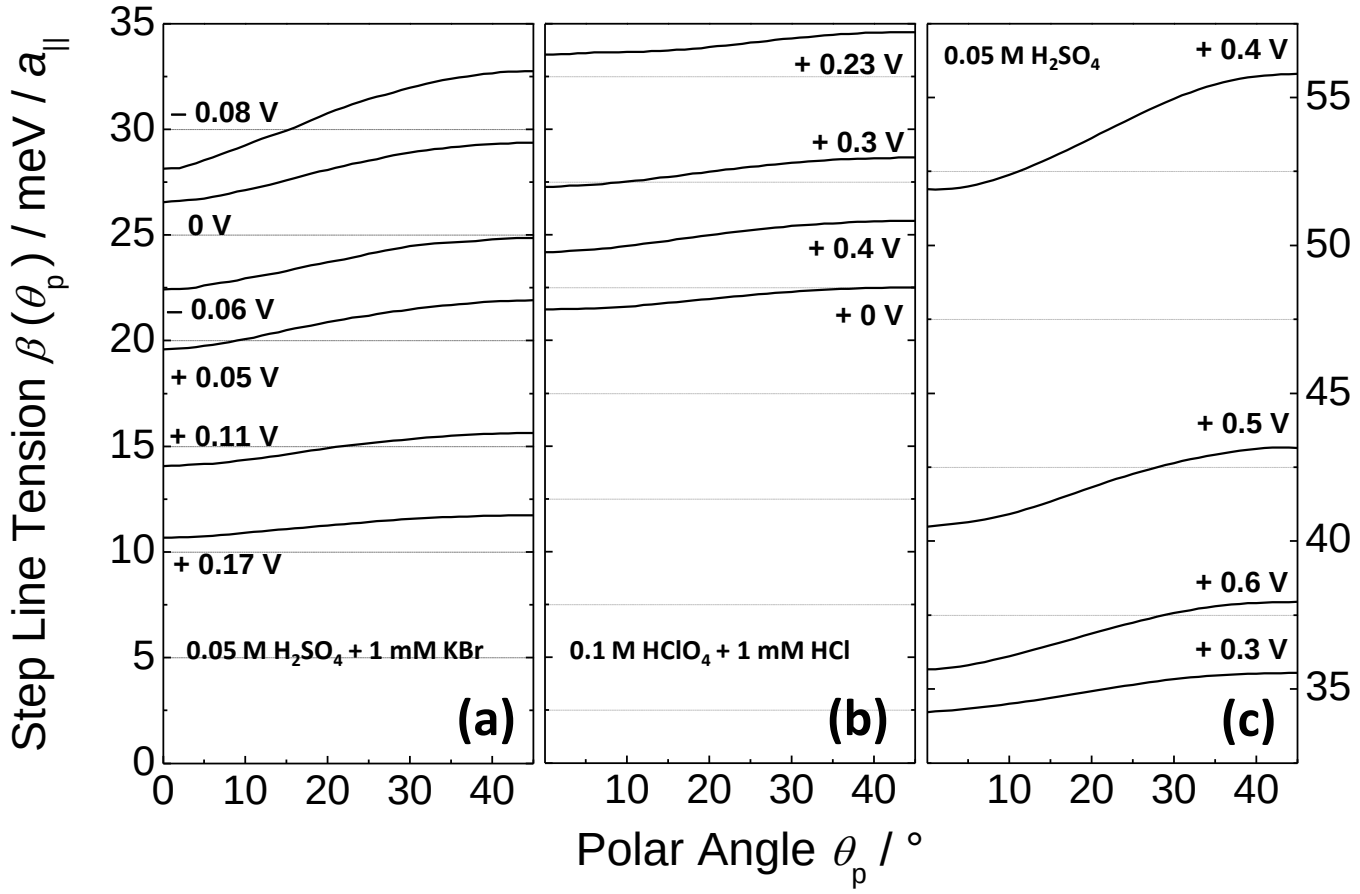

Fig. 6

Figure 7

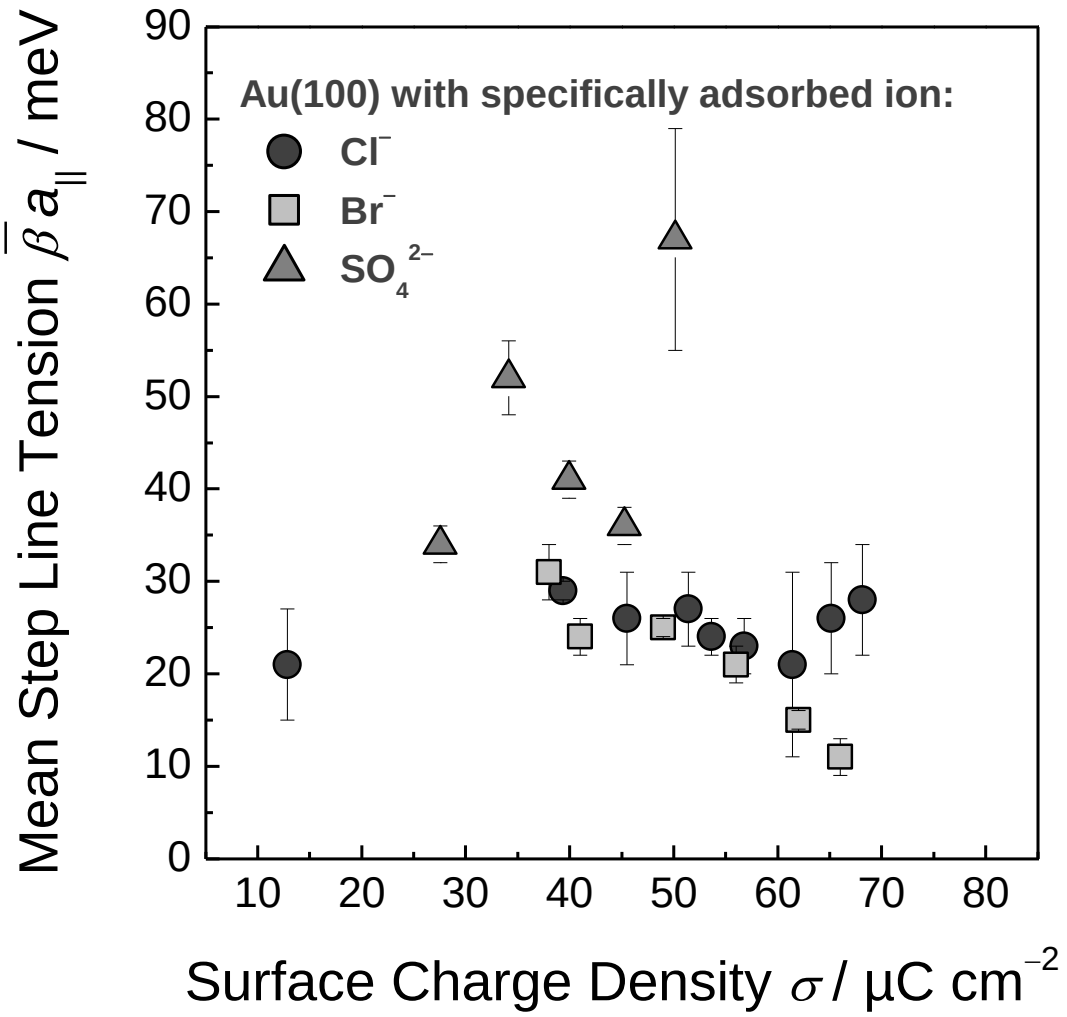

Fig. 7